Assessment of experimental optical techniques for characterizing heat transfer using numerical simulations

G.L. Juste[a]* and P. Fajardo[b]

[a]Aerospace Propulsion and Fluid Mechanics, Universidad Politécnica de Madrid, Plaza Cardenal Cisneros 3, 28040 Madrid, Spain; [b]Aerospace Engineering Group. Universidad Carlos III de Madrid, 28911 Leganés, Spain

(*Received 27 May 2014; final version received 19 November 2014*)

This manuscript addresses the application of numerical simulations for assessing the error in the measurement of the bulk temperature along the laser beam of a 3D flow using a 2D Moiré deflectometry analysis. To analyze the effect of different flow parameters on the error, a 3D computational model of an experimental system was developed. The simulated domain represents the well-known solution of the backward facing step in a rectangular channel but includes a hot-plate at the bottom of the step to enhance the heat transfer effects. The geometry resembles that found in a general heat exchanger. The difference between the computed bulk temperature of the flow and the average temperature obtained via the 2D Moiré is analytically evaluated for various assumed general temperature profiles; the numerically computed profiles of temperature indicates that the error decreases with the channel aspect ratio.

The use of CFD enables the determination of the flow topology and thus an evaluation of the 3D flow behavior that will cause the measurement error. A parametric study was performed for different flow conditions, namely, the aspect ratio of the channel, the inflow conditions (flow velocity or Reynolds number), and the temperature of the hot wall. The results indicate that the Moiré technique is suitable for evaluating the bulk temperature in typical heat exchange devices and flow conditions.

Keywords: Moiré deflectometry; error quantification; backward facing step; heat transfer

1. Introduction

The analysis of forced convection heat transfer in closed channels is a very interesting topic for many researchers because it is encountered in many applications, such as gas-turbine blade cooling, as can been seen in the works of Han (2004) and Tanda (2004), or the widely used plate-fin compact heat exchangers (Jang & Kim, 2005).

Moreover, the design of a high effectiveness heat exchanger requires high values of heat transfer area per unit volume, which is achieved by the use of narrow channels as a basic component of such systems (Sehgal, Murugesan, & Mohapatra, 2012). To maintain the pressure drops at a reasonable value, the flow velocity must be lowered, and this, together with the downsizing of passages, results in operation under laminar flow conditions (Chung, Tucker, & Roychowdhury, 2003).

In laminar flows, the effect of turbulence is negligible, and hence, the convective heat transfer coefficient is drastically reduced. To overcome this limit, pin fins inside the flow channel, with abrupt changes of the flow area, can promote turbulence to enhance the convective heat transfer rate (Togun, Kazi, & Badarudin, 2011). As consequence of this increment of area in the flow direction, flow separation and posterior reattachment might appear, and an adequate knowledge of the temperature field inside these closed channels is required for further optimization.

The availability of sophisticated numerical methods has not diminished the need for measurements, and experimental quantitative and qualitative observations are still required for developing a comprehensive phenomenological understanding of the flow-field phenomena and for validation of numerical models.

Different optical techniques have been developed and are commonly used in experimental heat transfer studies. A review of those techniques can be found in the literature in works of Merzkirch (1987) and Newport, Sobhan, and Garvey (2008). Due to the nonintrusivity of such optical techniques, which allows for obtaining local heat transfer data without influencing the investigated process, these techniques are well-suited for the verification of numerical results.

Among the existing optical techniques, those methods relying on the changes of the refractive index of the fluid, such as interferometry, holographic interferometry, or Moiré deflectometry, can be used in flows with uniform pressure to determine simultaneously the temperature field at every point of the selected spatial region. A comprehensive review of the advantages and disadvantages of different experimental techniques for the temperature measurement in flows has been presented by Shakher and Nirala (1999), Naylor (2003), Childs, Greenwood, and Long (2000) and Jordan, Tauscher, and Mayinger (1997).

These optical techniques are line-of sight methods, and therefore, they are influenced by the path of transmitted light, requiring the integration of the flow variables along the path. Consequently, the measurement of the refractive index gradient, or density gradient, distribution in the flow is straightforward only in the two-dimensional case and in the case of axisymmetric flow, by means of the Abel transform.

For a general three-dimensional field, a tomographic technique is applied to the two-dimensional fringe data obtained from multiple views to reconstruct the complete temperature field, as reported in Muralidhar (2012), Hirano, Kawaguchi, Satoh, and Saito (2006), and Michael and Yang (1992). However, there are configurations in which, due to the geometry, it is not possible to obtain several interferograms with different viewing angles, making the reconstruction impossible.

In applications in which the flow movement occurs mainly in one direction, such as the flow in rectangular closed channels, an alternative could be to obtain the two-dimensional bulk temperature in a plane parallel to the channel wall and the main direction of the flow. Obviously, this bulk temperature will depend on the velocity and temperature profiles in the plane perpendicular to the mainstream. These three-dimensional phenomena introduce errors on the bulk temperature measurement using two-dimensional techniques. The objective of this paper is to assess the effect of the flow variables on these errors. The amount of error is determined using CFD simulations to evaluate the difference between the beam-averaged and the bulk average temperature of the flow.

Several works in the literature report interferometric beam-averaged temperature and heat transfer data in a three-dimensional temperature field. For example, Naylor and Machin (2001) performed an investigation of beam-averaged temperature measurements in a three-dimensional field by the use of a two-dimensional analysis, but the measured average temperature did not agree with the defined bulk temperature. Juste and Benavides (2011) studied the end-wall errors in temperature measurement with Moiré deflectometry, but the technique was applied to external convective flow and mainly considered the edge effects only.

In the present work, the error produced when using two-dimensional Moiré deflectometry analysis to evaluate the bulk temperature of a three-dimensional internal flow is assessed. The analysis is performed in a closed rectangular channel that is straight and has a sudden expansion of flow area. This geometry is representative of many heat exchange applications and other engineering fields in which flow detachment and reattachment occur (Dufresne, Dewals, Erpicum, Archambeau, & Pirotton, 2011). The analysis is performed using a 3D-CFD numerical simulation of the laminar flow in the widely known backward facing step (BFS) channel configuration to provide a complete description of the expected flow topology, i.e., the velocity and temperature fields. The BFS configuration is commonly used as a benchmark for numerical analyses, and therefore, its solution is well known (Rajabi & Kavianpour, 2012). The heat transfer mechanism is modeled by a heated plate at the foot of the step. The effect of the parameters of the aspect ratio of the channel, the Reynolds number, the maximum temperature difference and the temperature distribution along the beam are analyzed.

2. Fundamentals of the laser Moiré deflectometry

To understand the error committed in the measurements due to the 3D flow phenomena, the basis of the experimental method should be reviewed first (as presented in Juste and Benavides, 2014). A drawing of a typical Moiré deflectometry configuration for temperature measurements in a backward-facing step is shown in Figure 1.

Moiré deflectometry obtains the ray deflections caused by the change of refractive index through phase objects. A parallel light beam passes, first, through the flow field, and then, through two identical gratings G1 and G2 separated by a pitch P and tilted an angle θ. Finally, the light reaches a screen, where an overlapped Moiré pattern is observed or registered with a camera.

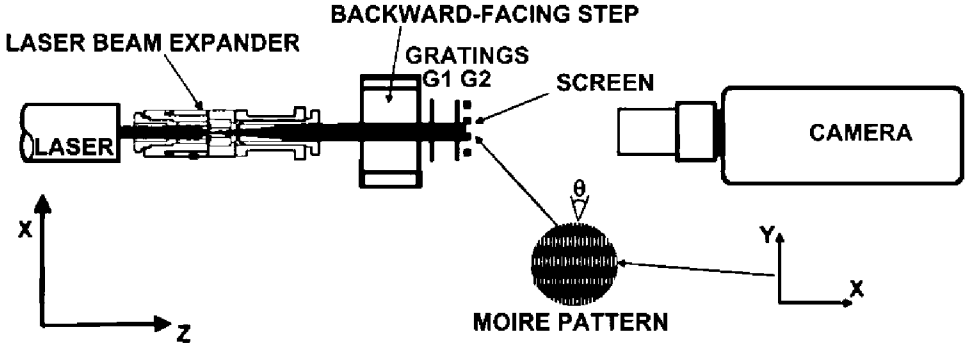

Figure 1. Diagram of the experimental procedure for Moiré deflectometry obtained from Juste and Benavides (2014).

If the flow field is uniform, a straight and unperturbed Moiré pattern with spatial period, P', of Moiré fringes is obtained. This unperturbed solution is given by:

$$P' = \frac{P}{2\sin(\theta/2)} \approx \frac{P}{\theta} \tag{1}$$

Disturbances in the flow induce a shift s at each point of the fringe and a deflection angle ϕ, which are linked with the refractive index n by means of the following system of equations:

$$\phi = \frac{1}{n_\infty}\int_o^L \frac{\partial n}{\partial y}dz \tag{2}$$

$$\phi = \frac{2s\,\sin(\theta/2)}{D} \tag{3}$$

The phase change φ of the Moiré pattern is also related to the displacement of the fringes and thus to the refractive index gradient. These dependencies are given by the following equations:

$$\varphi = \frac{2\pi s}{P'} \tag{4}$$

$$\varphi = \frac{2\pi D}{P}\frac{1}{n_\infty}\int_0^L \frac{\partial n}{\partial y}dz \tag{5}$$

If the flow field is two-dimensional, then the refractive index gradient in the fringe direction can be obtained as

$$\frac{\partial n}{\partial y} = \frac{Pn_\infty}{2\pi DL}\varphi \tag{6}$$

Applying the Gladstone–Dale law, the density can be obtained from the molar refractivity of the fluid in the following form:

$$n - 1 = K\rho \tag{7}$$

Considering the flow pressure to be constant, the temperature field can be calculated from the density field through the use of the ideal gas law, if the pressure and gas composition are known (R_g being the Gas Constant):

$$T = \frac{p}{R_g\rho} \tag{8}$$

An excellent theoretical review of refractive index mapping by Moiré deflectometry is presented in Kafri and Glatt (1990).

3. Evaluation of two-dimensional bulk temperature

In general, the movement of a fluid through a pipe or duct can be approximated to be *one-dimensional.* This means that the flow properties can be assumed to vary in the direction of flow only. As a result, all properties are assumed to be uniform at any cross-section normal to the flow direction, and the properties are assumed to have a *bulk average value* over the entire cross-section (Lienhard & Lienhard, 2000). The bulk average temperature is computed as:

$$T_b = \frac{\int_A \rho u c_P T dA}{\int_A \rho u c_P dA} \tag{9}$$

In this way, the energy flowing through a given cross-section is equal to $\dot{m}\bar{c}_p T_b$, where $\bar{c}_p$ is an average value. If all of the thermodynamic coefficients, e.g., c_P, are considered

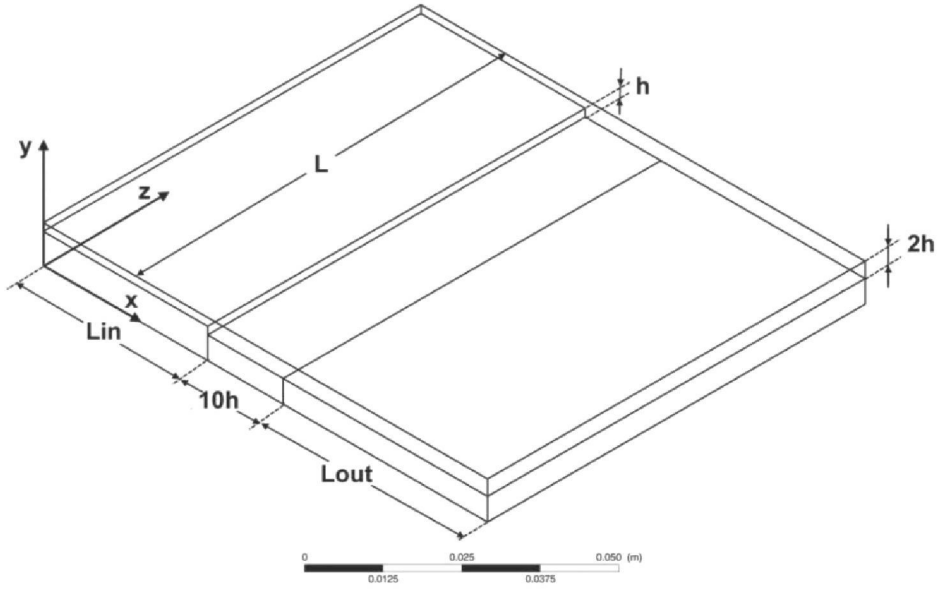

Figure 2. Sketch of the computational domain used in the simulations. The surface below the step (length 10 h) is heated.

to be constant, Equation (9) is reduced to

$$T_b = \frac{\int_A uTdA}{\int_A udA} \tag{10}$$

In a rectangular channel, as the one shown in Figure 2, the concept can be extended approximating the real flow to be two-dimensional, where the properties can be assumed to vary in the direction of flow (x axis) and in a perpendicular direction to the flow (y axis). The properties are then assumed to have *bulk average values* over the entire z-axis.

In this case, the bulk-averaged temperature along the z-axis is calculated as follows

$$T_b(x,y) = \frac{\int_{z_1}^{z_2} \rho(x,y,z)u(x,y,z)T(x,y,z)dz}{\int_{z_1}^{z_2} \rho(x,y,z)u(x,y,z)dz} \tag{11}$$

Considering the laser beam to be parallel to the z axis, the refractive index gradient averaged through the beam can be obtained as:

$$\left(\frac{\partial n}{\partial y}\right)_{2D} = \frac{1}{L}\int_{z_1}^{z_2} \frac{\partial n}{\partial y} dz \tag{12}$$

The refractive index is evaluated as:

$$(n)_{2D} = \overline{n_{ref}} + \int_{y_{ref}}^{y_2} \left(\frac{\partial n}{\partial y}\right)_{2D} dy \tag{13}$$

where $\overline{n_{ref}}$ is the average refractive index of refraction at the reference location y_{ref} and the 2D subscript in the previous expressions indicates that the magnitude is obtained from the Moiré analysis. The refractive index at any z-position along y-axis is related to the refractive index gradient by the following equation:

$$n = n_{ref} + \int_{y_{ref}}^{y_2} \frac{\partial n}{\partial y} dy \tag{14}$$

The average refractive index along z-axis can be expressed as:

$$\bar{n} = \frac{1}{L}\int_{z_1}^{z_2} n\, dz \tag{15}$$

Substituting Equation (14) into the integral in Equation (15), and then, applying Fubini's theorem and using Equation (12), gives

$$\bar{n} = \frac{1}{L}\int_{z_1}^{z_2} n_{ref}\, dz + \int_{y_{ref}}^{y_2} \left(\frac{\partial n}{\partial y}\right)_{2D} dy \tag{16}$$

The first term in Equation (16) is the average reference refractive index; therefore, the refractive index evaluated with 2D Moiré deflectometry analysis is the same as the average refractive index given by Equation (15).

Using the Gladstone–Dale relationship and Equation (15), the average temperature along the laser beam, obtained from 2D analysis of Moiré deflectometry and assuming constant pressure in the flow, is related to the temperature field, T(z), as follows

$$\bar{T} = \frac{L}{\int_{z_1}^{z_2} \frac{dz}{T(x,y,z)}} \tag{17}$$

The bulk average temperature computed in Equation (11) under the assumption of uniform pressure and ideal gas behavior, Equation (8), becomes

$$T_b(x,y) = \frac{\int_{z_1}^{z_2} u(x,y,z)dz}{\int_{z_1}^{z_2} \frac{u(x,y,z)}{T(x,y,z)}dz} \tag{18}$$

and for the hypothetical case of uniform velocity along the z-axis, Equation (17) becomes

$$T_b(x,y) = \frac{L}{\int_{z_1}^{z_2} \frac{dz}{T(x,y,z)}} \tag{19}$$

which is the same as the average temperature calculated from the 2D analysis of Moiré pattern, as stated in Equation (17). This means that under the previous hypothesis, the results will be the same. However, to achieve this result, some important assumptions have been made. In general, the average fluid temperature measured using 2D Moiré analysis is not equal to the bulk temperature along the light beam. The remaining part of this investigation is dedicated to assessing the magnitude of the difference between both temperatures and analyzing the main effects promoting this difference.

4. Numerical simulation

The problem tested numerically is a 3D steady laminar convective flow in a rectangular closed channel with a backward-facing step downstream. To solve the numerical problem, a commercial CFD package (ANSYS-Fluent) was used. The code is capable of solving the full Navier-Stokes equations in two-dimensional or three-dimensional geometries. For this purpose, the governing equations are discretized on a non-uniform Cartesian grid using a finite volumes procedure (Ansys, 2011). A second-order upwind scheme was used for the discretization of all of the equations to achieve higher-order accuracy (Moharana, Singh, & Khandekar, 2011; Singh, Paul, & Ranjan, 2011). A pressure-based solver was used. Pressure-velocity coupling was achieved using a SIMPLE (semi-implicit method for pressure-linked equations) algorithm, and the convergence was assured by using the default under-relaxation factors, as used in Singh et al. (2011) and Kim, Yadav, and Kim (2014). The convergence criterion used in the simulations requires that the residuals decrease by more than four orders-of-magnitude for all of the equations, with the exception of the energy equation, for which the criterion is to decreased by seven orders-of-magnitude.

Figure 2 shows the geometry of the rectangular duct and the backward-facing step used in this work along with

the proper the nomenclature and dimensions, similar to the one used by Juste and Benavides (2014) for an aspect ratio 50. The stream-wise length upstream of the step used in the presented study, L_{in} ($L_{in}/h = 21.76$), for Re $\leq$ 400 is larger or equal than the length obtained with the correlation provided by Durst, Ray, Ünsal, and Bayoumi (2005), who conducted a detailed numerical study and proposed a nonlinear correlation for laminar flow in two-dimensional channels given by:

$$L_{dl}/h = [(0.619)^{1.6} + (0.0567 \cdot \mathrm{Re})^{1.6}]^{1/1.6} \quad (20)$$

Furthermore, the velocity profiles along the y-axis obtained numerically at the step for all Reynolds numbers analyzed in this work are equivalent. This extra length ensures the full development of the flow along the y-axis in the duct before reaching the step.

The length of the channel behind the step, L_{out}, is selected to ensure that the outlet boundary condition does not affect the flow near the step. This selection is performed following the results of the work by Demuren and Wilson (1994), who demonstrated numerically that the flow field is not affected by increasing L_{out}/h beyond a value of 7.

To account for variations of temperature similar to the actual experimental configurations (Juste & Benavides, 2011), the heated surface behind the step with a length 10 h is an aluminum block (thermal conductivity = 180 W K^{-1} m^{-1}). The heater is a simple sheet resistor held to constant temperature under the aluminum block. The facing step and the bottom wall upstream of the step and downstream of the aluminum block are taken non-adiabatic (with a thermal conductivity equal to $k = 0.19$ W K^{-1} m^{-1}). Therefore, computation of thermal conduction through a solid material, coupled with heat transfer in fluid, was performed. This procedure, known as Conjugate Heat Transfer (CHT), is described in Ansys (2011). The top and sidewalls are assumed to be adiabatic.

The inlet flow condition consists in an air stream with uniform temperature, T_0, and velocity, u_0, profiles. A pressure condition was applied as the boundary condition at the exit plane (zero gauge pressure), which is located far downstream from the step to reduce the influence of the outflow conditions on the results. It was confirmed that the use of a longer computational domain did not change the flow behavior in the step region. On all solid walls, the no-slip boundary condition was applied.

Numerical simulations were performed for different values of free stream velocity u_0, resistor temperature (T_{hot}), and aspect ratio ($AR = L/h$), holding the height of the upstream duct and the expansion ratio (ER) of the step at a constant value. The Reynolds number characteristic of the flow behavior is based on the inlet velocity and the characteristic length D_h (hydraulic diameter = 2 h), which is in agreement with Armaly, Dursts, and Pereira (1983):

$$\mathrm{Re} = \frac{u_0 2\,h}{\nu}, \quad (21)$$

where the kinematic viscosity, ν, is evaluated for the air at the inlet temperature. A parametric study was performed to evaluate the effect of different variables. The main parameters used in the study are summarized in Table 1. As shown in Equation (20), both the inlet velocity and Reynolds number can be used to characterize the flow operation because they are equivalent parameters in this problem.

4.1. Grid independence

A mesh-independence analysis was performed to ensure the independence of the results; therefore, several quadrilateral meshes were considered. The velocity profiles in

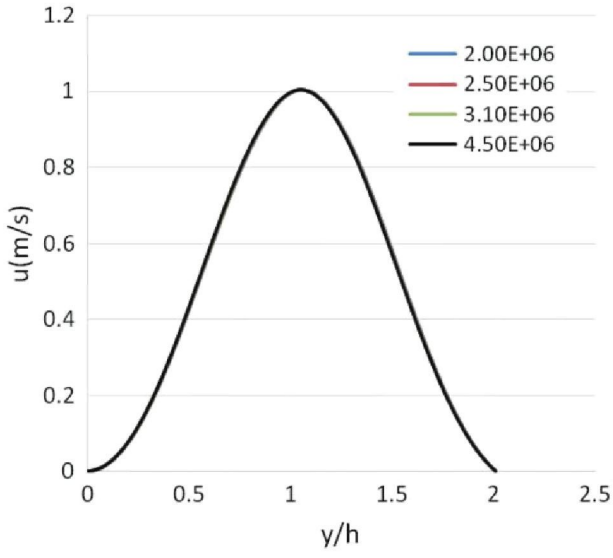

Figure 3. Velocity profiles at the center plane of the step and at x = 0.046 m.

Table 1. Parameters used in the simulations.

Geometrical parameters	Step height	h = 1.7 mm
	Expansion ratio	ER = 2
	Aspect ratio	$AR = \frac{L}{h} = \{50; 25; 12.5; 2.94; 1.47\}$
Operational conditions	Static pressure	P_0 = 101325 Pa
	Inlet temperature	T_0 = 293 K
	Inlet velocity	$u_0 = \{0.25\,\mathrm{m/s}; 0.5\,\mathrm{m/s}; 1\,\mathrm{m/s}; 2\,\mathrm{m/s}; 4\,\mathrm{m/s}\}$
	Corresponding Reynolds number	Re = {47.8; 95.7; 191.3; 382.7; 765.3}
	Resistor temperature	$T_{hot} = \{345\,\mathrm{K}; 400\,\mathrm{K}\}$

Table 2. Results of the mesh independence analysis.

Mesh number	Number of cells	E
1	$2.0{\cdot}10^6$	0.00975
2	$2.5{\cdot}10^6$	0.00614
3	$3.1{\cdot}10^6$	0.00452
4	$4.5{\cdot}10^6$	–

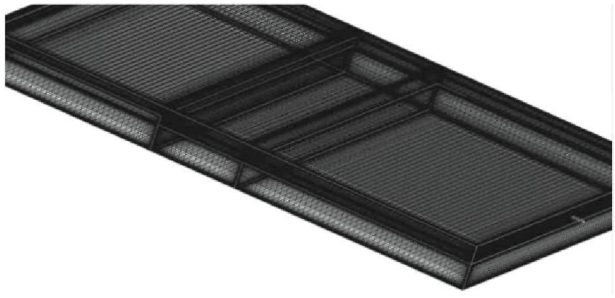

Figure 4. Computational mesh used in this work.

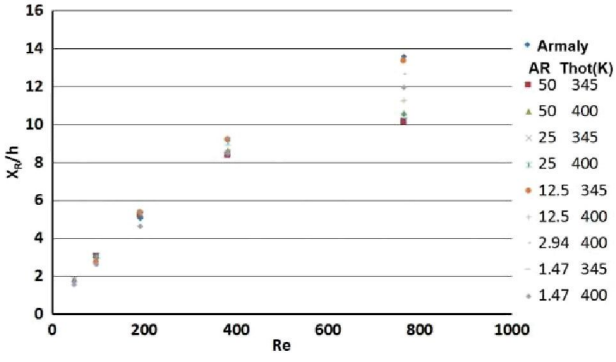

Figure 5. Reattachment length obtained in the simulations compared with the results presented in Armaly et al. (1983). The results correlate well up to a Reynolds number of 400.

the central plane of the step and at different x-positions for the case of Re = 226 were analyzed. As evidence, the results obtained at x = 0.046 m are shown below. Figure 3 presents the velocity profiles for at the center plane of the step and x = 0.046 m. All of the profiles appear to overlap into a single curve.

To provide a quantitative evaluation of the difference between the profiles, a similar procedure to the one described by Wang, Zhong, Zhang, and Kang (2014) is performed. The procedure is based on evaluating the root-mean-square error in the velocity, that is:

$$\varepsilon = \sqrt{\frac{1}{N}\sum_{i=1}^{N}\left(\frac{V_{i,n-1} - V_{i,n}}{V_{ave}}\right)^2} \tag{22}$$

where $V_{i,n-1}$ is the velocity in the former grid, $V_{i,n}$ is the velocity in the current grid, subscript I denotes the i^{th} sampling point, V_{ave} is the mean velocity of the profile, and N is the number of sampled points. The results are presented in Table 2.

The procedure was stopped at mesh number 3 because the root-mean-square error in the velocity was less than 0.5%.

Finally, a mesh with 3.1×10^6 grid cells was used in the computations in the case of the highest aspect ratio considered and a number of cells proportional to its volume in the rest of them. The region corresponding to the step is shown in Figure 4.

4.2. *Validation*

The accuracy of the numerical procedure was validated against the benchmarked experimental results of Armaly et al. (1983) by comparing the reattachment length in the mid-plane of z-axis. This parameter is the distance along the x-axis from the step corner to the point characterized by a zero longitudinal velocity in the extreme vicinity of the bottom wall.

The results obtained with the code ANSYS-Fluent for the different cases listed in Table 1 and for experimental results presented by Armaly are presented in Figure 5 and Table 3.

The agreement with the experimental results is good for Reynolds number values lower than 400 and for all of the aspect ratios analyzed. Moreover, one should remember that the results reported by Armaly et al. (1983) do not present an analysis of uncertainty evaluation. The disagreement found for higher Reynolds number values is

Table 3. Reattachment length.

			x_R/s								
	Armaly	AR	50		25		12.5		2.94	1.47	
Re		T_{hot} (K)	345	400	345	400	345	400	400	345	400
47.83	1.75		1.82	1.84	1.83	1.86	1.8	1.71	1.87	1.61	1.56
95.66	2.98867806		3.07	3.09	3.08	3.12	2.74	3.08	3.05	2.63	2.65
191.32	5.05126073		5.22	5.29	5.24	5.3	5.37	5.39	5.26	4.64	4.65
382.65	8.41018554		8.37	8.65	8.51	9.02	9.21	9.29	8.62	8.45	8.46
765.31	13.588147		10.13	10.62	10.2	10.5	13.3	11.3	12.7	11.2	12

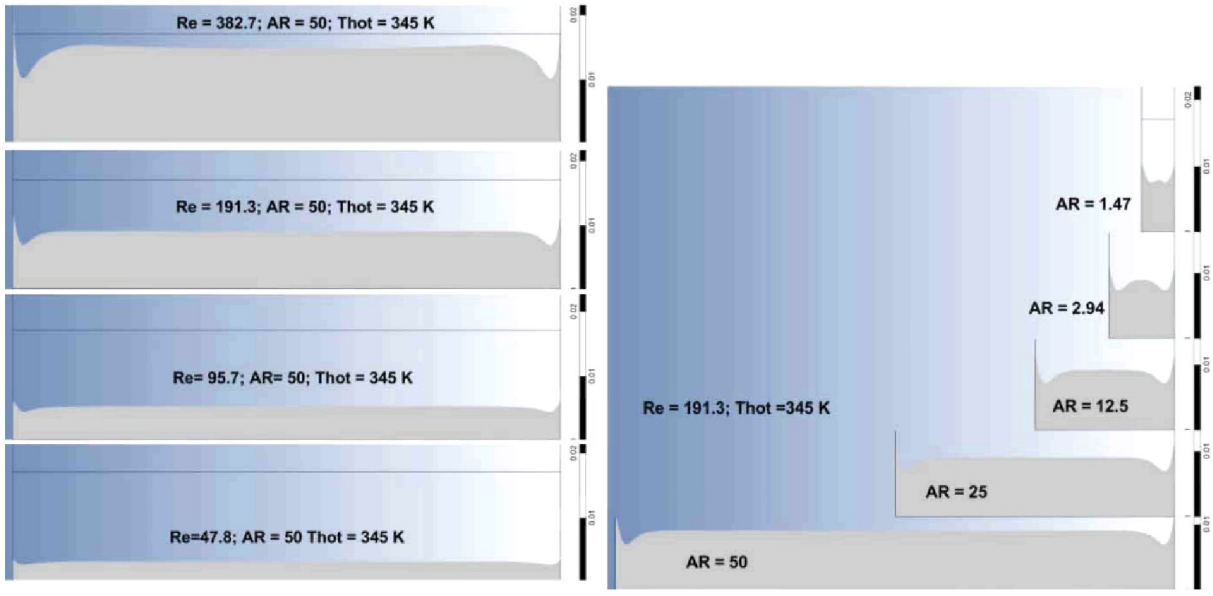

Figure 6. Variation of the reattachment length in the span-wise direction for different Re (left) and aspect ratios, AR, of the channel (right).

explained by the fact that the numerical simulation was performed assuming laminar flow and steady state conditions, but it is known that as the Reynolds number increases, the flow becomes turbulent. In the experiments performed by Armaly et al. (1983), the regime of laminar to turbulent transition was found in the range of Reynolds number of 1200–6600, but the actual representative range can be lower, as was shown in the works of Mouza, Pantzali, Paras, and Tihon (2005) and Tihon, Pěnkavová, Havlica, & Šimčík (2011). Other works, such as Kaiktsis, Karniadakis, and Orszag (1991) and Beaudoin, Cadot, Aider, and Eduardo Wesfreid (2004), studied the turbulent transition and the appearance of turbulent instabilities in the BFS geometry. Those results demonstrated that if an unstable turbulent region embedded in the surrounding laminar flow survives in the stream-wise direction, then the outflow plane cuts through this structure, and the accuracy of predicted profiles is strongly influenced by the outflow boundary condition.

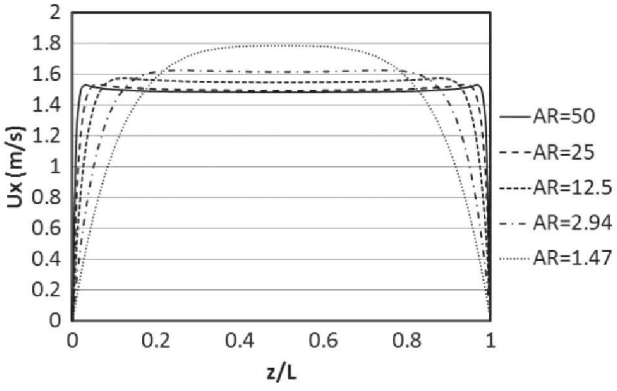

Figure 7. Variation of the span-wise velocity profiles at the mid-plane y of the channel with the aspect ratio (AR).

The discrepancies with the experimental data of Armaly et al. (1983) are attributed to the onset of three-dimensionality due to the turbulence for Reynolds

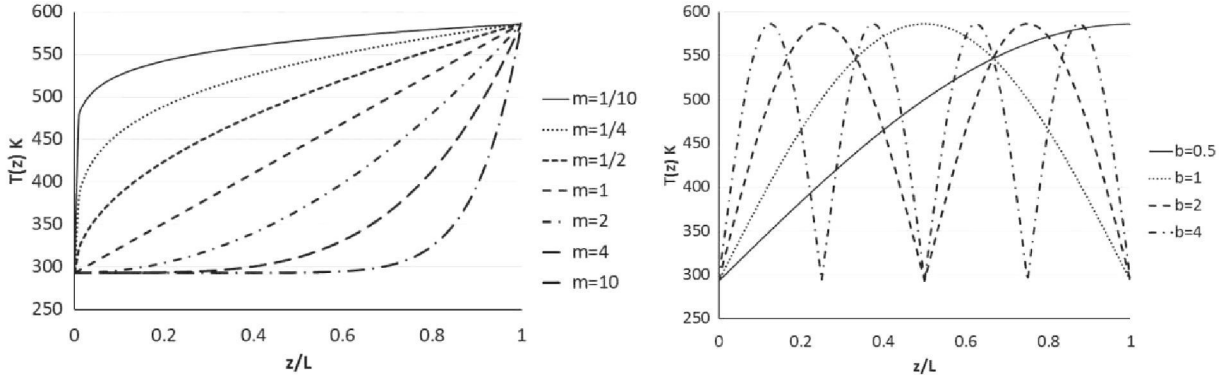

Figure 8. Different temperature profile shapes considered in this work. The panel figure represents different temperature profiles assuming a power-law shape (Equation (23)), while the right panel illustrates the temperature profile as a periodic function.

number values exceeding 600. Kaiktsis et al. (1991) identified a bifurcation of two-dimensional laminar flow to three-dimensional flow at Re = 700 as the primary source of mismatch between the simulation and the experimental data.

Moreover, the span-wise flow that develops adjacent to the side wall in the region close to the step modifies the reattachment length of 3D flow, as shown in Figure 6. The numerical simulation was performed for the full width in the z-axis instead of using a symmetry plane to represent a real experiment. The boundary represented in Figure 6 consists of the points in the span-wise direction, where the longitudinal velocity in the proximity of the bottom wall is zero, i.e., the onset of separation. Figure 6 (left) shows the variations with the Reynolds number and Figure 6 (right) shows the variation with aspect ratio.

The results show a similar behavior to those obtained in the work of Barbosa et al. (2005) and Beaudoin et al. (2004). The minimum x_R value of the reattachment line is located near the side walls, and the maximum is exactly on the side walls, while the central section of the curve is approximately constant (except for small aspect ratios). The three-dimensional effects increase as the Reynolds number increases and represent a larger extent of the span-wise width when decreasing the aspect ratio.

5. Discussion

5.1. *Results in the channel upstream the step*

Before analyzing the flow downstream of the step, we first studied the flow in the rectangular channel upstream of it at axial location $x/h = 14$. Span-wise direction velocity profiles for different aspect ratios are presented in Figure 7.

Although the distance from the inlet section was selected to ensure the full development of the flow in the y-direction, this does not occur in the span-wise direction. For large aspect ratios, the span-wise velocity distribution is close to a uniform velocity profile. When decreasing the aspect ratio, the velocity profile approaches the fully developed flow.

5.2. *Importance of the temperature profile*

To evaluate the importance of the temperature profile shape on the difference between the average Moiré temperature and the two-dimensional bulk temperature along the laser beam in closed rectangular channels, different hypothetical shapes of temperature profiles were considered, i.e., power functions with varying exponents:

$$T = T\left[1 + \left(\frac{z}{L}\right)^m\right] \tag{23}$$

such as those shown in Figure 8 (left) or periodic functions with varying frequencies:

$$T = T_{ref}\left\{1 + \left|\sin\left(\pi b \frac{z}{L}\right)\right|\right\} \tag{24}$$

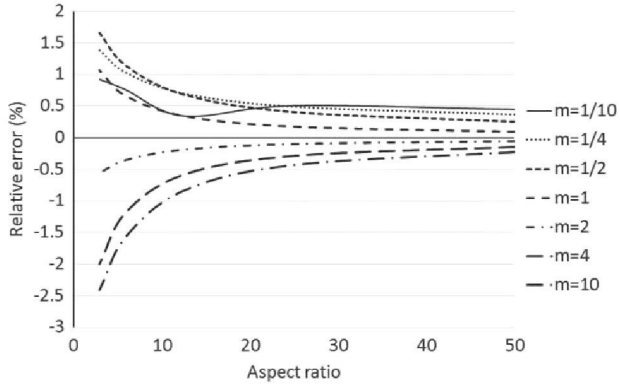

Figure 9. Relative error between the bulk and two-dimensional Moiré temperature as a function of the channel aspect ratio and for different exponents in the assumed temperature distribution (power-law Equation (23)).

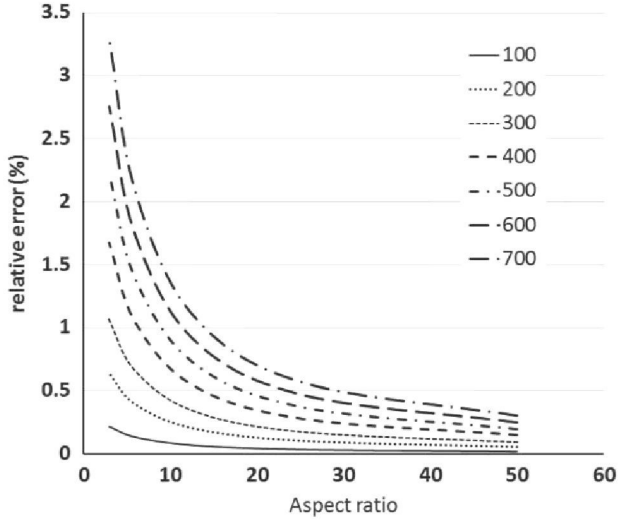

Figure 10. Relative error between the bulk and two-dimensional Moiré temperature as a function of the channel aspect ratio and for different ΔT (assuming a linear temperature distribution).

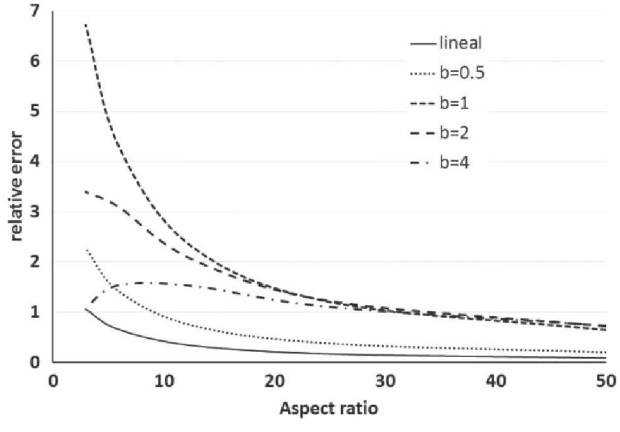

Figure 11. Relative error in the determination of the bulk temperature using a 2D Moiré analysis as a function of the channel aspect ratio and for different frequencies in the assumed temperature distribution (periodic function, Equation (24)).

as presented in Figure 8 (right). The former group represents temperature profiles close to a hot wall surface, while the latter group can simulate a heat exchanger with periodic fins. Figure 9 shows the relative error between bulk temperature and two-dimensional Moiré temperature with respect to the channel aspect ratio, assuming a power-law distribution of flow temperatures with different exponents and $\Delta T = (T_{max}\text{-}T_{min}) = 293$ K.

From the results, it is clear that, in addition to the small errors due to numerical integration, the temperature error is always small, that is, lower than 0.5, for aspect ratios larger than 20, which is obviously due to a nearly uniform velocity profile in the duct (see Figure 7). As the aspect ratio decreases, the velocity profile approaches a fully developed profile, the three dimensional effects arise, and the temperature error increases. This increment

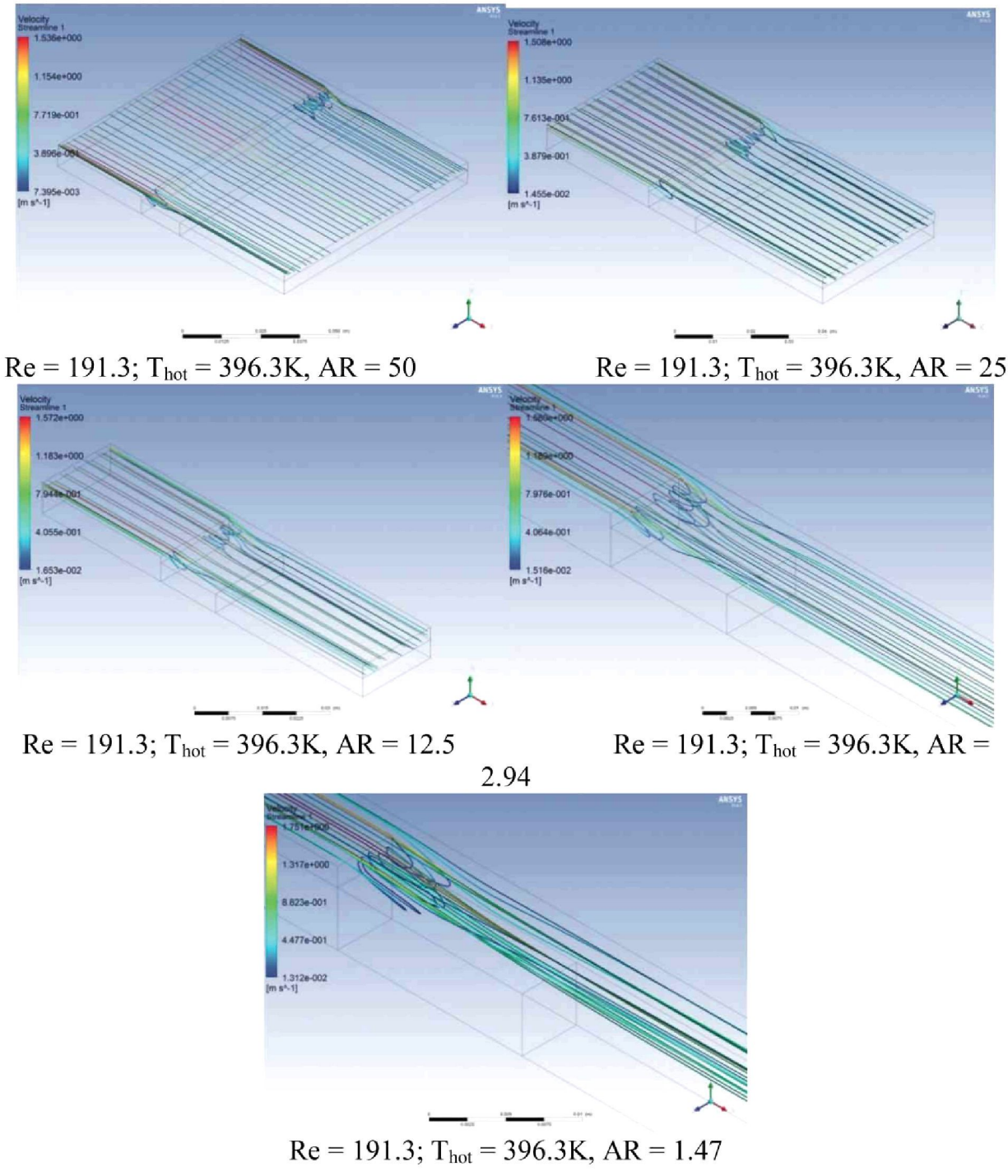

Figure 12. Streamlines after the backward-facing step for different channel aspects ratios.

in the relative error is higher as the exponent of the assumed power-law distribution deviates from the linear behavior. In any case, the error is relatively small for any value of the exponent of the power distribution of temperature.

The flow maximum temperature difference selected for computations, ΔT, is an overall limit for most heat exchanger applications. Figure 10 shows the variation of error with the aspect ratio for several values of ΔT and for the exponent, $m = 1$. The error in the estimation of bulk

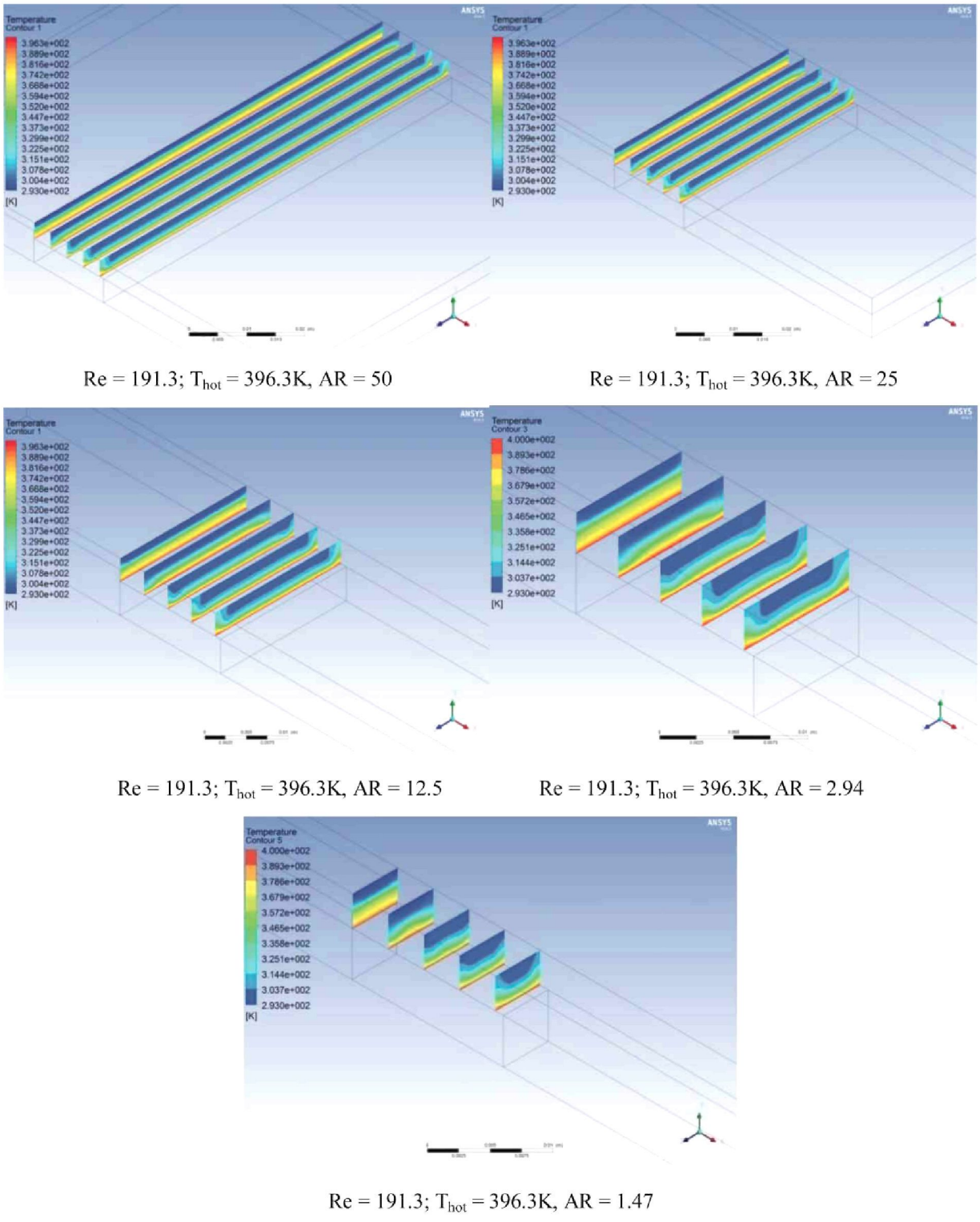

Re = 191.3; T_{hot} = 396.3K, AR = 50

Re = 191.3; T_{hot} = 396.3K, AR = 25

Re = 191.3; T_{hot} = 396.3K, AR = 12.5

Re = 191.3; T_{hot} = 396.3K, AR = 2.94

Re = 191.3; T_{hot} = 396.3K, AR = 1.47

Figure 13. Temperature field in several y–z planes after the step.

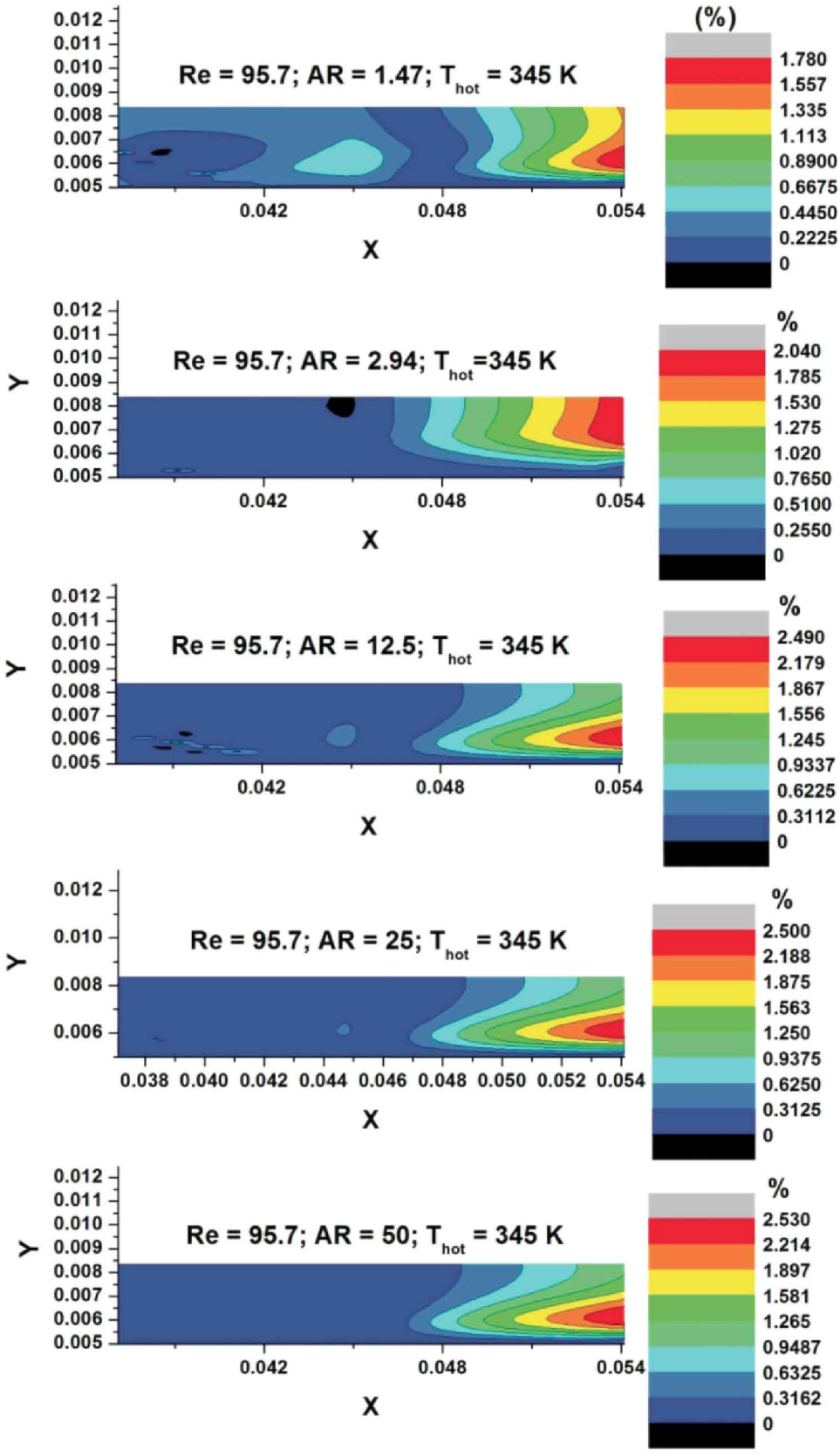

Figure 14. Error in the evaluation of the bulk temperature: effect of the aspect ratio (AR).

temperature is observed to increase with the temperature difference; this error can be of importance (more than a 1%) for aspect ratios lower than 10, i.e., with a velocity profile fully developed.

The results for the case of periodic temperature distribution are illustrated in Figure 11. Just as the case of the power-law distribution, the error in temperature estimation is small, below 1%, for aspect ratios larger than 20, i.e., for velocity profiles approximately uniform. When increasing the frequency, the error decreases. This behavior occurs because as the temperature profile approaches a uniform distribution, as derived from Equation (16) and Equation (18), and when the temperature distribution is uniform, the bulk temperature and the two-dimensional Moiré temperature are the same, as was previously demonstrated.

From these theoretical cases, the importance of 3D effects can be understood. It is possible to conclude that the relative error is reduced as the aspect ratio decreases and that the error is as small as a 3% for aspects ratios higher than 10 for all of the temperature profiles considered.

5.3. *Results after the step*

Rectangular ducts are basic components of cooling systems, but the main focus of the current work is on flow configurations with real three-dimensional features. The backward facing step allows for the study of the three-dimensional aspects of flows with separation and subsequent reattachment caused by a sudden change in the channel geometry. Next to a backward facing step, the swirling flow appearing in the span-wise direction, developed adjacent to the stepped wall, modifies the reattachment region of this separated-reattached three-dimensional flow, and consequently, the heat transfer downstream of the step, as shown in Rani, Sheu, and Tsai (2007).

Features of the three-dimensional laminar flow adjacent to the backward-facing step for changing aspect ratios are shown in Figure 12. The figure shows how the streamlines near the sidewall take different paths as they flow downstream from the step, leading to swirling flow in the span-wise direction inside the recirculation region. A similar result was obtained in the works of Nie and Armaly (2002, 2003). As the aspect ratio decreases, the portion of the flow governed by the vortex increases, until it represents the full width of backward facing step (AR $\approx$ 1.5).

The temperature distribution in span-wise direction is also influenced by the three-dimensional behavior of flow. Figure 13 shows the temperature distribution in several yz-planes after the step for different aspect ratios.

The three-dimensional behavior of the temperature field increases as the flow moves downstream, and it also represents a larger extent of the flow in the span-wise direction, mainly far from the bottom wall, as the aspect ratio decreases.

The following figures are representative samples of the error in the evaluation of bulk temperature using 2D Moiré analysis in the cases listed in Table 1. As a rule of thumb, it can be established that the errors are small (less than 5%) for all of the studied cases in the region

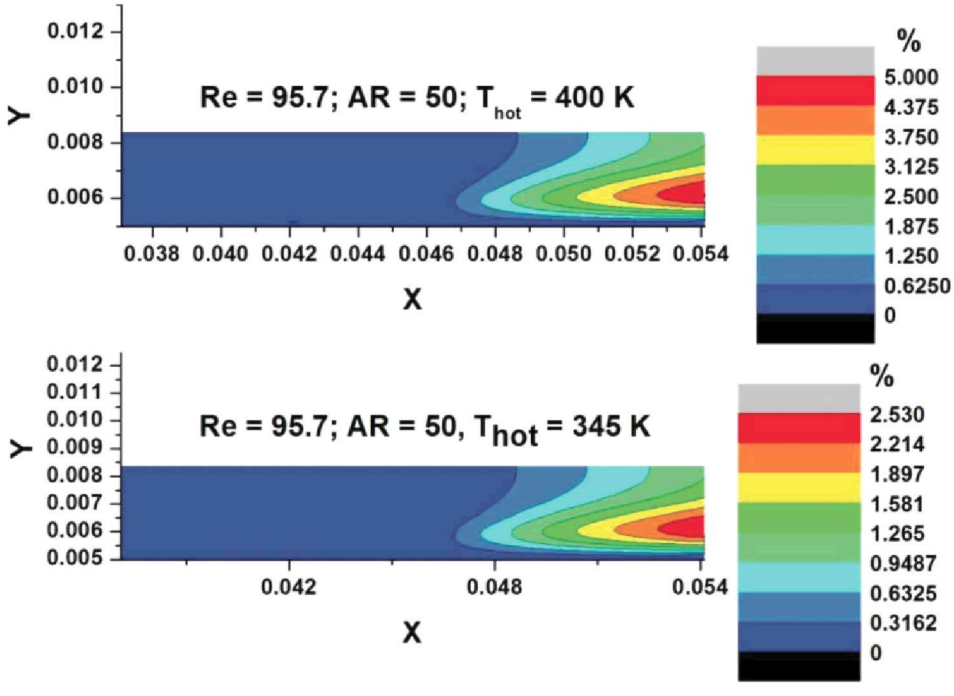

Figure 15. Error in the evaluation of the bulk temperature: effect of the resistor temperature (T_{hot}).

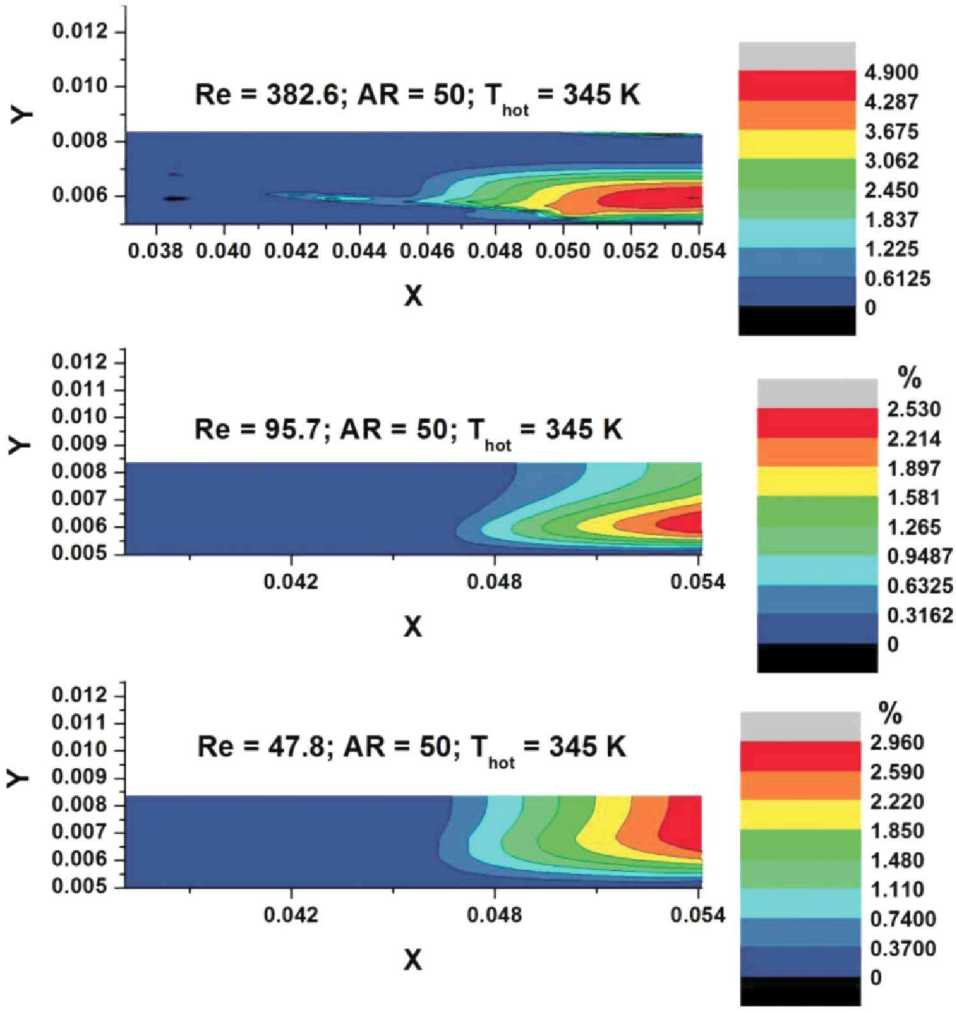

Figure 16. Error in the evaluation of the bulk temperature: effect of the Reynolds number (Re).

close to the step. The figures represent the error field in the region immediately downstream of the step covering the heated length (10 h). The y axis covers a range from 5 to 8.4 mm (2 h), and the magnitudes are established in a manner that reproduces the geometry used in the work of Juste and Benavides (2014). The maximum is found at the end of the heated plate and approximately at the central point.

Separating the effect of the different parameters, the influence of aspect ratios is analyzed in Figure 14. For a Re of 95.7 and with the resistor temperature at the smallest value considered in this analysis, $T_{hot} = 345$ K, the maximum error obtained is approximately 2.5%. As the aspect ratio decreases, the discrepancy between the 2D Moiré and the actual bulk temperature increases, probably due to the vortex flow in span-wise direction.

The effect of the temperature difference between the heated plate (bottom wall) and the flow is presented in Figure 15. The shape of the error fields are quite similar, but the magnitude of the error increases with temperature, mainly in the region downstream, where the three-dimensional effects in temperature are more relevant. This result agrees with the results of a previous study performed in the rectangular channel upstream of the step.

Finally, the effect of the Reynolds number, which is equivalent to the stream-wise inlet velocity, on the evaluation of bulk temperature agrees with that shown in Equation (17). Increasing the Reynolds number increases the inlet velocity, and therefore, the error in the evaluation of bulk temperature is also increased. These results are presented in Figure 16.

6. Conclusions

The main interest in using optical techniques for flow measurements is their non-intrusivity, which allows for obtaining the main characteristics of the flow without influencing the investigated process. This work focused on one of these techniques, namely, Moiré deflectometry, which is a line-of-sight technique in which a collimated laser beam

is used to measure the optical properties of the inspected flow domain. The technique is particularly suited for the heat transfer measurements, such as the one required in heat exchange applications.

In this work, an analysis of the error introduced when measuring the bulk flow temperature along the laser beam using a 2D Moiré deflectometry analysis was presented. First, the process of evaluating the flow temperature using this technique was described in the paper, and an analytical estimation of the error for different temperature profiles along the laser beam was performed, indicating that the error decreases with the aspect ratio for the different profiles.

The analysis was performed by means of numerical simulations on the flow in the well-known geometry of the backward facing step in a rectangular channel, in which the bottom wall is heated to introduce the heat transfer effects. This geometry represents a simplified geometry of a general heat exchanger. A parametric analysis of the error was performed for different aspect ratios of the channel, different inlet Reynolds numbers (or inlet velocities) and different temperatures of the hot plate. The values were chosen as characteristic values for general heat exchanger applications. The simulations were previously validated against the benchmarked experimental results from the literature, finding good agreement for the different operating conditions. The difference between the experimental results and the simulations increases with the increase in the Reynolds number. This effect can be attributed to the onset of turbulent transition on the flow. The use of CFD allows for the recovery of the full flow field description. From the velocity and temperature fields, it is clear that the 3D effects increase as the aspect ratio decreases.

In conclusion, from the estimated 2D error field obtained via numerical simulation, the bulk temperature can be closely approximated using a two-dimensional Moiré analysis because the error is less than 5% (but increases with T_{hot}). The maximum error increases also with the increasing Reynolds number (or inlet velocity). However, the variation with the aspect ratio is less effective. Therefore, the Moiré technique is suitable for evaluating the bulk temperature in typical devices and flow conditions encountered in heat exchangers, with strong three-dimensional effects, but with a driving flow direction.

Nomenclature

A	cross section area
AR	aspect ratio (L/h)
c_P	specific heat at constant pressure
D	distance between gratings
D_h	hydraulic diameter
ER	expansion ratio (H/h)
G1, G2	gratings
g	gravity constant
h	height of the step
H	height of the channel
K	Gladstone-Dale constant
L	width of the backward facing step
L_{in}	channel length before the step
L_{dl}	development length
L_{out}	channel length after the step
n	refractive index
N	number of samples
P	distance between two grating lines
P'	distance between two fringes
p	pressure
p_0	inlet fluid pressure
Re	Reynolds number
R_g	gas constant
T	temperature
T_b	bulk temperature
T_{hot}	hot wall temperature
T0	inlet fluid temperature
s	fringe shift
u	fluid velocity in the x direction
u_0	free stream velocity
V	Velocity
x,y,z	Cartesian coordinates
x_R	reattachment length
ϵ	mean root-square velocity error
ϕ	deflection angle of the rays lights
φ	phase change of Moiré pattern
ν	kinematic viscosity
θ	angle between gratings
ρ	density

ORCID

G.L. Juste http://orcid.org/0000-0002-7663-9084
P. Fajardo http://orcid.org/0000-0002-0531-8021

References

Ansys. Ansys Fluent User's Guide Fluent Inc. (2011, November). *Release 14.0*. Ansys, Southpointe, Canonsburg, PA.

Armaly, B. F., Dursts, F., & Pereira, J. C. F. (1983). Experimental and theoretical investigation of backward-facing step flow. *Journal of Fluid Mechanics*, *127*, 473–496.

Beaudoin, J. F., Cadot, O., Aider, J. L., & Eduardo Wesfreid J. (2004). Three-dimensional stationary flow over a backward-facing step. *European Journal of Mechanics-B/Fluids*, *23*(1), 147–155.

Childs, P. R. N., Greenwood, J. R., & Long, C. A. (2000). Review of temperature measurement. *Review of Scientific Instruments*, *71*(8), 2959–2978.

Chung, Y. M., Tucker, P. G., & Roychowdhury, D. G. (2003). Unsteady laminar flow and convective heat transfer in a sharp 180° bend. *International Journal of Heat and Fluid Flow*, *24*(1), 67–76.

Demuren, A., & Wilson, R. (1994). Estimating uncertainty in computations of two-dimensional separated flows. *Journal of Fluids Engineering*, *116*, 216–220.

Dufresne, M., Dewals, B., Erpicum, S., Archambeau, P., & Pirotton, M. (2011) Numerical investigation of flow patterns in rectangular shallow reservoirs. *Engineering Applications of Computational Fluid Mechanics*, *5*(2), 247–258.

Durst, F., Ray, S., Ünsal, B., & Bayoumi, O. A. (2005). The development lengths of laminar pipe and channel flows. *Journal of Fluids Engineering*, *127*(6), 1154–1160.

Han, J. C. (2004). Recent studies in turbine blade cooling. *International Journal of Rotating Machinery*, *10*(6), 443–457.

Hirano, T., Kawaguchi, T., Satoh, I., & Saito, T. (2006, June 1–10). *Non-intrusive temperature measurement of curved surface using laser interferometer and computer tomography*. Proceedings of 13th International Symposium on Applications of Laser Techniques to Fluid Mechanics.

Jang, S. P., & Kim, S. J. (2005). Fluid flow and thermal characteristics of a microchannel heat sink subject to an impinging air jet. *Journal of Heat Transfer*, *127*(7), 770–779.

Jordan, M., Tauscher, R., & Mayinger, F. (1997). New challenges in thermo-fluid dynamic research by advanced optical techniques. *International Journal of Heat and Technology*, *15*(1), 43–54.

Juste, G. L., & Benavides, E. M. (2011). End-wall errors in temperature measurement of external convective heat transfer with Moire deflectometry. *Optics and Lasers in Engineering*, *49*, 8–12.

Juste, G. L., & Benavides, E. M. (2014). Moiré-Fourier deflectometry for local heat transfer measurement over a backward-facing step. *International Journal of Thermal Sciences*, *77*, 244–251.

Kaiktsis, L., Karniadakis, G. E., & Orszag, S. A. (1991). Onset of three-dimensionality, equilibria, and early transition in flow over a backward-facing step. *Journal of Fluid Mechanics*, *231*, 501–528.

Kafri, O., & Glatt, I. (1990). *The physics of Moiré metrology*. New York: John Wiley.

Kim, J., Yadav, M., & Kim, S. (2014). Characteristics of Secondary Flow Induced by 90-Degree Elbow in Turbulent Pipe Flow. *Engineering Applications of Computational Fluid Mechanics*, *8*(2), 229–239.

Lienhard, J. H., & Lienhard, J. (2000). *A heat transfer textbook*. Cambridge: Phlogiston Press.

Merzkirch, W. (1987). *Flow visualization* (2nd ed.). San Diego: Academic Press.

Michael, Y. C., & Yang, K. T. (1992). Three-dimensional Mach-Zehnder interferometric tomography of the Rayleigh-Bénard problem. *Journal of Heat Transfer*, *114*(3), 622–629.

Mouza, A. A., Pantzali, M. N., Paras, S. V., & Tihon, J. (2005). *Experimental and numerical study of backward-facing step flow*. 5th National Chemical Engineering Conference. Thessaloniki, Greece.

Moharana, M. K., Singh, P. K., & Khandekar, S. (2011, January). *Axial heat conduction in the context of developing flows in microchannels*. ASME 2011 9th International Conference on Nanochannels, Microchannels, and Minichannels.

Muralidhar, K. (2012). Temperature field measurement in buoyancy-driven flows using interferometric tomography. *Annual Review of Heat Transfer*, *12*, 265–375.

Naylor, D., & Machin, A. D. (2001). The accuracy of beam averaged interferometric temperature measurement in a three-dimensional field. *Experimental Heat Transfer*, *14*, 217–228.

Naylor, D. (2003). Recent developments in the measurement of convective heat transfer rates by laser interferometry. *International Journal of Heat and Fluid Flow*, *24*, 345–355.

Newport, D., Sobhan, C. B., & Garvey, J. (2008). Digital interferometry: techniques and Trends for Fluid Measurement. *International Journal of Heat and Mass Transfer*, *44*, 535–546.

Nie, J. H., & Armaly, B. F. (2002). Three-dimensional convective flow adjacent to backward-facing step-effects of step height. *International Journal of Heat and Mass Transfer*, *45*(12), 2431–2438.

Nie, J. H., & Armaly, B. F. (2003). Reattachment of three-dimensional flow adjacent to backward-facing step. *Journal of Heat Transfer*, *125*(3), 422–428.

Rajabi, E., & Kavianpour, M. R. (2012). Intelligent prediction of turbulent flow over backward-facing step using direct numerical simulation data. *Engineering Applications of Computational Fluid Mechanics*, *6*(4), 490–503.

Rani, H. P., Sheu, T. W., & Tsai, E. S. (2007). Eddy structures in a transitional backward-facing step flow. *Journal of Fluid Mechanics*, *588*, 43–58.

Barbosa, J. G. S., Sarin, V., & Anand, N. K. (2005). Numerical simulation of mixed convective flow over a three-dimensional horizontal backward facing step. *Journal of Heat Transfer*, *127*(9), 1027–1036.

Shakher, C., & Nirala, A. K. (1999). A review on refractive index and temperature profile measurements using Laser-based interferometric techniques. *Optics and Lasers in Engineering*, *31*, 455–491.

Sehgal, S. S., Murugesan, K., & Mohapatra, S. K. (2012). Effect of channel and plenum aspect ratios on the performance of microchannel heat sink under different flow arrangements. *Journal of Mechanical Science and Technology*, *26*(9), 2985–2994.

Singh, A. P., Paul, A. R., & Ranjan, P. (2011). Investigation of reattachment length for a turbulent flow over a backward facing step for different step angle. *International Journal of Engineering, Science and Technology*, *3*(2), 84–88.

Tanda, G. (2004). Heat transfer in rectangular channels with transverse and V-shaped broken ribs. *International Journal of Heat and Mass Transfer*, *47*(2), 229–243.

Tihon, J., Pěnkavová, V., Havlica, J., & Šimčík, M. (2012). The transitional backward-facing step flow in a water channel with variable expansion geometry. *Experimental Thermal and Fluid Science*, *40*, 112–125.

Togun, H., Kazi, S. N., & Badarudin, A. (2011). A review of experimental study of turbulent heat transfer in separated flow. *Australian Journal of Basic and Applied Sciences*, *5*(10), 489–505.

Wang, Y., Zhong, K., Zhang, N., & Kang, Y. (2014) Numerical analysis of solar radiation effects on flow patterns in Street Canyons. *Engineering Applications of Computational Fluid Mechanics*, *8*(2), 252–262.